PHD2 Constrains Antitumor CD8$^+$ T-cell Activity

Charlotte Bisilliat Donnet[1,2], Valérie Acolty[1,2], Abdulkader Azouz[3,2], Anaëlle Taquin[1,2], Coralie Henin[1,2], Sarah Trusso Cafarello[4], Sébastien Denanglaire[1,2], Massimiliano Mazzone[4,5], Guillaume Oldenhove[1,2], Oberdan Leo[1,2], Stanislas Goriely[1,3,2], and Muriel Moser[1,2]

ABSTRACT

The prolyl hydroxylase domain/hypoxia-inducible factor (PHD/HIF) pathway has been implicated in a wide range of immune and inflammatory processes, including in the oxygen-deprived tumor microenvironment. To examine the effect of HIF stabilization in antitumor immunity, we deleted *Phd2* selectively in T lymphocytes using the cre/lox system. We show that the deletion of PHD2 in lymphocytes resulted in enhanced regression of EG7-OVA tumors, in a HIF-1α–dependent manner. The enhanced control of neoplastic growth correlated with increased polyfunctionality of CD8$^+$ tumor-infiltrating lymphocytes, as indicated by enhanced expression of IFNγ, TNFα, and granzyme B. Phenotypic and transcriptomic analyses pointed to a key role of glycolysis in sustaining CTL activity in the tumor bed and identified the PHD2/HIF-1 pathway as a potential target for cancer immunotherapy.

Introduction

Since the discovery of tumor-specific and tumor-associated antigens in the nineties (1), numerous studies (2) have demonstrated that the immune system can constrain tumor development in humans and rodents. However, several sequential steps are required for effective tumor control *in vivo*, and these are subject to negative feedback mechanisms. These steps include priming in the draining lymph nodes, migration to the tumor bed, reactivation in the tumor microenvironment, and tumor lysis. It is clearly established that the tumor microenvironment displays several features that determine the outcome of immune reactivity to tumor cells. Among them, hypoxia (low oxygen tension) is a common characteristic of most solid tumors and may impede antitumor immunity by regulating the function and/or recruitment of various immune cell types.

Cell adaptation to hypoxia is regulated via a set of oxygen sensors, among which members of the oxygen-dependent prolyl hydroxylase family [prolyl hydroxylase domain (PHD) or EGLN], comprising 3 members, play a major role. Hypoxia-inducible factors (HIF), of which there are three (HIF-1α, HIF-2α, and HIF-3α), are a set of evolutionary conserved transcriptional regulators that represent the best-characterized substrates of PHDs (3). These transcription factors are active as heterodimers consisting of a cytoplasmic HIF (mostly HIF-1α and/or HIF-2α) subunit and a nuclear HIF-1β subunit also known as ARNT (aryl hydrocarbon receptor nuclear translocator). Both subunits are constitutively expressed by all mammalian cells studied to date. Under normoxic conditions, HIFα is hydroxylated on two prolines by one of the 3 members of the PHD family, leading to its poly-ubiquitination by the E3 ubiquitin ligase complex VHL (composed of Von Hippel-Lindau protein, elongin B and C, Cullin 2 and Rbx1) and in its degradation by the proteasome (4). Under hypoxic conditions, PHD enzymes are inhibited and unable to hydroxylate the HIFα subunit, which can then bind to the HIFβ subunit and activate and/or inhibit the expression of over 1,000 genes (3).

The impact of hypoxia on immune reactivity in the tumor microenvironment has been studied using direct and indirect (through stabilization of HIF) approaches. A number of reports suggest that hypoxia may sustain tumor progression by (i) triggering the protumoral function of macrophages entrapped in hypoxic niches (5); (ii) recruiting other immunosuppressive cell types, such as myeloid-derived suppressor cells and regulatory T cells (Treg; ref. 6); (iii) downregulating Th1-type cell activation (7–10); and (iv) favoring Th17 differentiation (11, 12). The effect of hypoxia on Treg remains controversial: depending on the study and model considered, HIF-1α, the major oxygen sensor stabilized during hypoxia, has been shown to repress the Treg transcriptional program *in vitro* by inducing the degradation of Foxp3 (11, 12), or to favor their differentiation and function in a murine model of inflammatory bowel disease (13). Hypoxia may also promote immune evasion by inducing HIF-1α–dependent expression of immune checkpoint proteins (14, 15). In addition, hypoxia displays intrinsic effects on tumor cells, promoting the expression of genes that induce epithelial–mesenchymal transition, affect cell adhesion, and drive cancer development in the case of long-lasting HIF signaling (16–19). By contrast, there is increasing evidence that enhanced HIF activity may potentiate the cytotoxic activity of CD8$^+$ T lymphocytes, which are major actors of antitumor immunity. Doedens and colleagues showed that loss of VHL (the main regulator of HIF stability) led to enhanced control of persistent viral infection *in vivo* and that VHL-deficient OT-I CTLs displayed a superior capacity to control ovalbumin (OVA)-expressing melanoma upon transfer (20). Hypoxic conditions *in vitro* increase the production of the cytolytic molecule granzyme B in a HIF-1α–dependent manner (21, 22).

These observations highlight the contrasting role of proteins involved in hypoxia sensing in the regulation of immunity/tolerance in the tumor microenvironment and raise the question of its global

[1]Laboratory of Immunobiology, Université Libre de Bruxelles, Gosselies, Belgium. [2]U-CRI (ULB Center for Research in Immunology), Université Libre de Bruxelles, Gosselies, Belgium. [3]Institute for Medical Immunology, Université Libre de Bruxelles, Gosselies, Belgium. [4]Laboratory of Tumor Inflammation and Angiogenesis, Center for Cancer Biology, VIB, Leuven, Belgium. [5]Laboratory of Tumor Inflammation and Angiogenesis, Center for Cancer Biology, Department of Oncology, KU Leuven, Leuven, Belgium.

C. Bisilliat Donnet, V. Acolty, and A. Azouz contributed equally as co–first authors of this article.

S. Goriely and M. Moser contributed equally as co–last authors of this article.

Corresponding Author: Muriel Moser, Department of Molecular Biology, ULB Cancer Research Center, Université Libre de Bruxelles, 10 rue Adrienne Bolland, Gosselies 6041, Belgium. Phone: + 32 486 30 39 56; E-mail: Muriel.Moser@ulb.be

Cancer Immunol Res 2023;11:339–50

doi: 10.1158/2326-6066.CIR-22-0099

pro- or antitumoral role. In this study, we used mice genetically deficient for *PHD2* (a proline-hydroxylase that mediates control of HIF activity) selectively in T lymphocytes ($PHD2^{\Delta T}$) to characterize the phenotype and function of tumor-infiltrating $CD8^+$ T lymphocytes in mice displaying elevated HIF-1 activity selectively in T lymphocytes.

Materials and Methods

Mice

C57BL/6 mice were purchased from Envigo (Horst, the Netherlands). C57BL/6 *Phd2*$^{flox/flox}$ mice were generated as previously described (23, 24) and kindly provided by Dr. Bart Lambrecht (Ghent University). C57BL/6 *Hif1α*$^{flox/flox}$ (B6.129-Hif1atm3Rsjo/J) mice were kindly provided by Dr. F. Bureau (Université de Liège) and CD4 Cre (B6.Cg-Tg(Cd4-cre)1Cwi/BfluJ) mice by Dr. G. Van Loo (Ghent University). Mice carrying *Hif1α* and *Egln1* (*Phd2*) loxP-flanked alleles were crossed with CD4 Cre mice to obtain T cell–specific gene deletion. Mice were housed in individual ventilated cages and used at 6 to 9 weeks of age. The experiments were performed in compliance with the relevant laws and institutional guidelines and were approved by the Animal Care and Use Committee of the Institute for Molecular Biology and Medicine (protocol numbers: CEBEA-IBMM-2017–22–01 and 03).

Tumor inoculation and *in vivo* treatment

EG7-OVA (source: ATCC CRL-2113) T lymphoblasts are derived from the C57BL/6 (H-2^b) mouse lymphoma cell line EL4, which was transfected by electroporation with the plasmid pAc-neo-OVA which carries a complete copy of chicken OVA mRNA and the neomycin (G418) resistance gene. B16-OVA (clone MO4, kindly provided by Kris Thielemans, VUB, Belgium) is a cell line that was isolated from skin tissue of a mouse with melanoma and was transfected with chicken OVA cDNA. It exhibits a morphology of spindle-shaped and epithelial-like cells. No full authentication was carried out, but the EG7-OVA cell line was characterized by T-cell markers; the B16-OVA cell line displays morphologic characteristics (see above), both cell lines were evaluated for SIINFEKL OVA/K^b expression using 25-D1.16 mAb (eBioscience 17–5743–82).

EG7-OVA and B16-OVA tumor cell lines were cultured in DMEM (Lonza 12–741F) containing 10% heat-inactivated FCS (Gibco 10270–106), sodium pyruvate 1 mmol/L (Lonza 13–115E), 1% nonessential aminoacid mixture (Lonza 13–114E), L-glutamine 2 mmol/L (Lonza BE17–605E), penicillin–streptomycin 100 units/mL (Lonza DE17–6025E), β-mercaptoethanol 50 μmol/L (Sigma-Aldrich M-7522) and G418 400 μg/mL (Sigma-Aldrich A1720). Tumor cell medium was changed every 2 days and a new cell line was regenerated every month. Cell lines were treated every 6 months with Mycoplasma Removal Reagent (Millipore 30–500–44).

10^6 EG7-OVA tumor cells were injected subcutaneously in the right flank. Mice were monitored every 2 days for tumor growth and survival. The tumor volume (mm^3) is expressed as $(A \times B^2)/2$, where A and B are tumor length and width, respectively. Some mice were injected intraperitoneally with 1-mg anti-CD8β (53–5.8, BioXCell BE0223) or IgG from rat serum (Sigma-Aldrich I8015) 5 days after tumor inoculation, and further treated with 250 μg antibodies weekly.

5×10^5 B16-OVA tumor cells were injected subcutaneously in the right flank. Some mice were injected intraperitoneally with 200–280 μg anti–programmed cell death protein 1 (PD-1; RMP1–14, BioXCell BP0146) or isotype control (rat IgG2a, 2A3, BioXCell BE0089) 7, 9, 11, and 13 days after tumor inoculation.

Cell culture

$CD8^+$ T lymphocytes were positively selected from spleen suspensions by magnetic-activated cell sorting using CD8 beads (Miltenyi 130–117–044) according to the manufacturer's protocol.

For transcriptomic analysis, enriched $CD8^+$ T lymphocytes were stained with anti-TCRβ and anti-CD8 mAbs and further purified using a BD FACSAria III Cell Sorter. Sorted $CD8^+$ T lymphocytes were activated with plate-bound anti-CD3 (2 μg/mL; clone: 145–2C11; BioXCell) and soluble anti-CD28 (1 μg/mL, clone: 37.51; BioXCell) in RPMI1640 medium (Gibco 31870–025) containing 10% FCS, sodium pyruvate, nonessential amino acid mixture, L-glutamine, penicillin–streptomycin, and β-mercaptoethanol.

To measure glucose dependency, MACS-enriched $CD8^+$ T lymphocytes were cultured with DMEM medium without glucose (Life Technologies 11–9660–25) supplemented with 10 mmol/L glucose (Sigma-Aldrich G8270) or galactose (Sigma-Aldrich G5388) and 10% dialyzed FCS, sodium pyruvate, nonessential amino acid mixture, L-glutamine, penicillin–streptomycin, and β-mercaptoethanol.

Flow cytometry

EG7-OVA tumors were treated with DNAse I (Roche 10104159001) and Liberase (Roche 05401020001) to generate a single-cell suspension and viable cells were enriched on density gradient Lymphoprep (Stemcell Technologies 07851). Tumor-infiltrating cells were incubated with monoclonal antibodies conjugated to fluorochrome or biotin: TCRβ (H57–597), CD8α (53–6.7), CD44 (IM7), CD62 L (MEL-14), TIGIT (1G9), CD279/PD-1 (J43), TIM-3 (5D12) from BD Biosciences. Streptavidin was purchased from BD Bioscience (557598). Dead cells were excluded by LIVE/DEAD (Invitrogen L34976) staining and nonspecific Fc-mediated interactions were blocked by anti-mouse CD16/CD32 (2.4G2, BioXCell). To evaluate the functional status of tumor-infiltrating T lymphocytes, cells were stimulated *in vitro* for 3 hours with pharmacologic agents bypassing TCR signaling (50 ng/mL PMA (Sigma P8139) and 1 μg/mL ionomycin (Sigma I 0634) in the presence of a protein trafficking inhibitor allowing the intracellular retention of activation-induced cytokines (brefeldin A from Invitrogen 00–4506–51). Cells were subsequently fixed with BD cytofix/cytoperm kit (51–2090KZ), permeabilized with BD Perm/Wash (51–2091KZ) and stained with conjugated monoclonal antibodies directed at IFNγ (XMG1.2, Biolegend), Granzyme B (NGZB, Thermo Fisher), TNFα (MP6-XT22, Life Technologies), Ki67 (B56, BD Bioscience), T-bet (4B10, Thermo Fisher), Eomes (DAN11MAG, Thermo Fisher), Glut-1 (SPM498, Abcam), TOX (TXRX10, Thermo Fisher), and/or TCF1/TCF7 S33–966, BD Pharmingen). The expression of a transcription factor cascade (Tox, TCF1, T-bet, Eomes) was used to define four exhausted PD-1^+CD8^+ T lymphocyte subsets, in particular the terminally exhausted subset $TCF1^-T\text{-}bet^{lo}Tox^{hi}Eomes^{hi}$ (25).

Flow cytometry analysis was performed on a Canto II (BD Biosciences) or CytoFLEX (Beckman Coulter) and the data generated were analyzed using the FlowJo software (Tree Star) and the FlowSOM technique. This visualization technique analyzes flow or mass cytometry data using a self-organizing map (26).

In vivo CTL assay

C57BL/6 mice were immunized by injection of dendritic cells pulsed with SIINFEKL peptide (synthesized by PEPTIDE.2). Spleen cells were digested with collagenase type 3 (Gestimed LS004183) for 30 minutes

at 37°C, further dissociated in Ca^{2+}-free medium, and separated into low and high density fraction on a Nycodenz gradient (LUCRON 1002424). $CD11c^+$ cells were enriched from low-density spleen cells by magnetic positive selection using anti-CD11c (N418) Microbeads (Miltenyi 130–108–338). Dendritic cells were incubated for 1 hour at 37°C with SIINFEKL peptide, washed and suspended in 200 μL PBS. 5×10^5 SIINFEKL-pulsed dendritic cells were injected into the hind and fore footpads. Mice were tested 5 days later.

For the *in vivo* CTL assay, naïve or immunized mice were injected intravenously with target cells. Target cells were splenocytes from C56BL/6 mice pulsed or not with 5 μg/mL SIINFEKL peptide and further labeled with 5,6-carboxyfluorescein diacetate succinimidyl ester (CFSE, Molecular Probes C-1157) at a concentration of 10 μmol/L (pulsed) and 1 μmol/L (unpulsed) for 15 minutes at 37°C. Target cells were washed and injected intravenously at 1:1 ratio (total of 4×10^5 cells). Draining lymph nodes were harvested 6 hours later and analyzed by flow cytometry to determine the number and proportion of $CFSE^+$ cells. The percentage of antigen-specific lysis *in vivo* was calculated as follows:

$$\left(1-\frac{\left(\frac{\#\ cells\ CFSE\ high}{\#\ cells\ CFSE\ low}\right)}{\left(\frac{\#\ cells\ CFSE\ high\ from\ naive\ mice}{\#\ cells\ CFSE\ low\ from\ naive\ mice}\right)}\right)*100$$

Quantitative RT-PCR

RNA was extracted from $CD8^+$ T lymphocytes (purified by cell sorting) using TRIzol method (Sigma-Aldrich T9424) and reverse transcribed with Superscript II reverse transcriptase (Invitrogen 18064–014) according to the manufacturer's instructions. Quantitative real-time RT-PCR was performed using the SYBR Green Master mix kit (Thermo Fisher, K1082) and StepOne Plus system (Applied Biosystems). Amplification reactions were conducted for 40 PCR cycles (each cycle: 95C for 15 seconds, 60C for 1 hour) in duplicates. The following RT PCR primers were used: Ubiq-Fw: cgtctgaggggtggctatta; Ubiq-Rev: taaattggggcaagtggcta; Glut-1-Fw: caaacttcattgtgggcatg; Glut-1-Rev: agcaccgtgaagatgatgaa; Sprouty 2-Fw: cgatcacggagttcagatgt; Sprouty 2-Rev: agctctggcctccatcag. Transcript amounts were calculated by using a standard curve and normalized to Ubiquitin-transcripts, which was used as the housekeeping gene.

RNA sequencing and analysis

$CD8^+$ T lymphocytes, purified as indicated in the "cell culture" section of the methods, were stimulated with anti-CD3 and anti-CD28 antibodies for 15 hours. RNA extraction was performed using a RNeasy kit (Qiagen, 74004) and sample quality was tested on a 2100 Bioanalyzer (Agilent). Total RNA underwent paired-end sequencing by using a TruSeq Stranded mRNA kit (25×106 paired-end reads/sample, Novaseq 6000 platform) performed by BRIGHTcore ULB-VUB, Belgium (http://www.brightcore.be). Adapters were removed with Trimmomatic-0.36 (with the following parameters: Truseq3-PE.fa:2:30:10 LEADING:3 TRAILING:3 SLIDINGWINDOW:4:15 MINLEN:36 HEADCROP:4). Reads were then mapped to the reference genome mm10 by using STAR_2.5.3 a software with default parameters. Reads were then sorted from the alignment according to chromosome positions and index the resulting BAM-files. Read counts in the alignment BAM-files that overlapped with the gene features were obtained using HTSeq-0.9.1 with "–nonunique all" option (if the read pair aligns to more than one location in the reference genome, it was counted in all features to which it was assigned and scored multiple times). Genes with no raw read count greater or equal to 20 in at least 1 sample were filtered out with an R script, raw read counts were normalized and a differential expression analysis was performed with DESeq2 by applying an adjusted P value < 0.05 and an absolute log2-ratio larger than 0.5.

Statistical analysis

All statistical analyses were conducted using GraphPad Prism (GraphPad Software, version 6). Statistical difference between two groups was determined by unpaired, two-tailed Student t tests. A one-way or two-way ANOVA was used for multigroup comparisons together with Tukey multiple comparisons *post hoc* tests.

Survival significance in tumor bearing mice was determined by a Log-rank Mantel–Cox test. Data are judged to be statistically significant when P value < 0.05. In figures, asterisks denote statistical significance (*, $P < 0.05$; **, $P < 0.01$; ***, $P < 0.001$; ****, $P < 0.0001$).

Data availability

The RNA sequencing (RNA-seq) data reported in this study have been deposited in the Gene Expression Omnibus repository with the accession code no. GSE216536. All other data are available in the main text or the Supplementary Materials or are available from the corresponding author on reasonable request.

Results

Genetic deletion of *phd2* in T lymphocytes results in enhanced tumor rejection

To explore the role of the HIF pathway in the adaptive response to tumor *in vivo*, we deleted the gene encoding PHD2 selectively in T cells and monitored the growth of EG7-OVA lymphoma cells. Mice with *lox*P-flanked *Egln1* (*Phd2*) alleles [generated as previously described (23, 24)] were crossed onto CD4 Cre mice, giving rise to the $Egln1^{fl/fl}$ $CD4^{CRE}$ (named $PHD2^{\Delta T}$) mouse strain harboring a selective deletion of *Egln1* (*Phd2*) in T lymphocytes. Expression of HIF-1α was increased in $CD8^+$ T cells upon 24h *in vitro* stimulation with anti-CD3/CD28 (Supplementary Fig. S1A). We subcutaneously injected EG7-OVA lymphoma cells into $PHD2^{\Delta T}$ mice and compared tumor growth with that seen in wild-type (WT) mice and control littermates ($CD4\ Cre^-$ $Phd2^{fl/fl}$). The data in **Fig. 1A** indicate that a significant proportion of $PHD2^{\Delta T}$ mice (mean = 67% in all experiments performed) rejected the tumor and survived at endpoint, as compared with 2.6% in WT mice. The tumor growth in $Phd2^{fl/fl}$ was slower than in WT mice, presumably due to altered, hypomorphic expression of the floxed *Phd2* allele (**Fig. 1S**, panel B). Of note, deletion of HIF-1α in otherwise PHD2-deficient mice (HIF-1α $PHD2^{\Delta T}$) reverted the phenotype, as assessed by the control-like survival rate of these mice upon tumor inoculation (**Fig. 1A** and **B**). The control of tumor growth was dependent on $CD8^+$ T lymphocytes, as the injection of depleting anti-CD8 increased mortality in both WT and $PHD2^{\Delta T}$ mice (**Fig. 1C** and **D**). Administration of anti-CD4 resulted in reduced tumor growth and death, presumably because of Treg depletion (Supplementary Fig. S2). Similar results, i.e., enhanced tumor regression, were observed in $PHD2^{\Delta T}$ mice injected with B16-OVA melanoma (**Fig. 2**, see isotype-treated groups). Thus, stabilization of HIF-1α resulted in increased control of tumor growth in two murine models.

Genetic deletion of *Phd2* favors the development of effector $CD8^{\pm}$ T cells

To examine whether the *Phd2* deletion affected the differentiation of $CD8^+$ T lymphocytes into effector and/or memory cells, we used flow

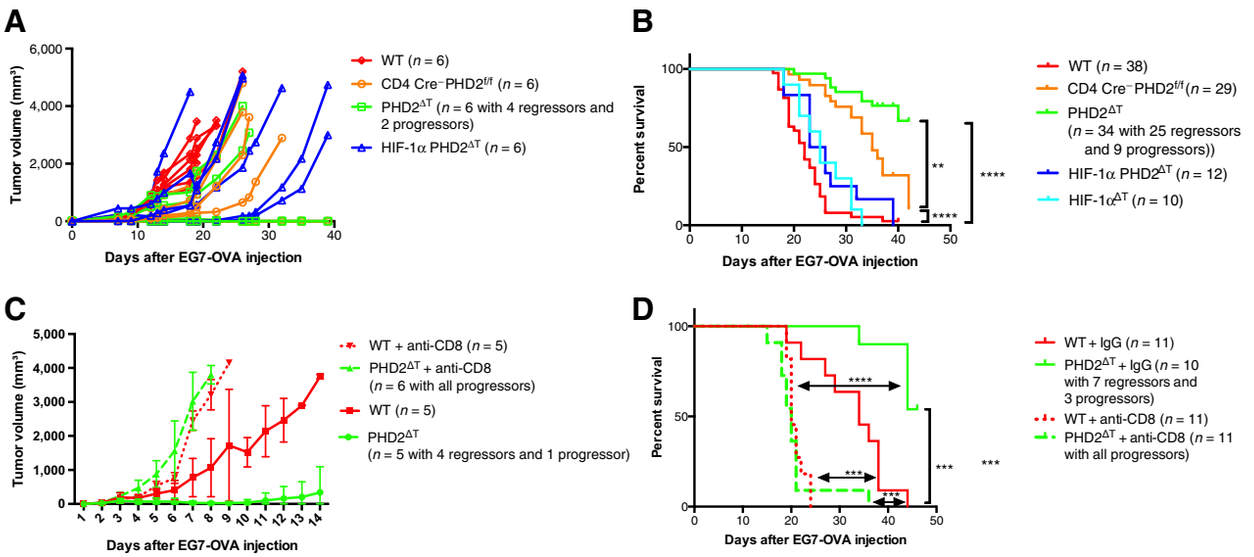

Figure 1.
Enhanced tumor regression in PHD2$^{\Delta T}$ mice. **A**–**D**, Mice were injected subcutaneously with 10^6 EG7-OVA tumor cells. **C** and **D,** Some groups were treated 5 days later with rat depleting anti-CD8 or isotype control IgG. Tumor growth (**A**, **C**) and survival (**B**, **D**) were monitored daily. Data are representative of two ($n = 3$–6; **A**); at least three ($n = 3$–8) for WT, CD4 Cre$^-$ PHD2$^{f/f}$, PHD2$^{\Delta T}$ groups and two ($n = 3$–8) for HIF-1α PHD2$^{\Delta T}$ and HIF-1α$^{\Delta T}$ groups (**B**); one (**C**); two ($n = 5$–6; **D**) independent experiments. **A**, **C**, Bars represent mean ± SD. Statistical significance was determined by the Mann–Whitney test. *, $P < 0.05$; **, $P < 0.01$; ***, $P < 0.001$; ****, $P < 0.0001$; ns, not significant.

cytometry to monitor the capacity (upon PMA/ionomycin restimulation) of tumor-infiltrating CD8$^+$ T lymphocytes to express IFNγ, TNFα, and Granzyme B as well as the glucose transporter GLUT-1, a direct target of HIF-1α. We used FlowSOM (self-organizing map) as a starting point for an analysis of a pool of cells from 4 experimental groups. Six major clusters were identified, from which two populations (identified as POP 1 and 2) were strongly enriched selectively in PHD2$^{\Delta T}$ mice (Supplementary Fig. S3). We split the data set to visualize the proportion of the populations in the four experimental groups (**Fig. 3A** and **B**). The expression of IFNγ, TNFα, and GLUT-1

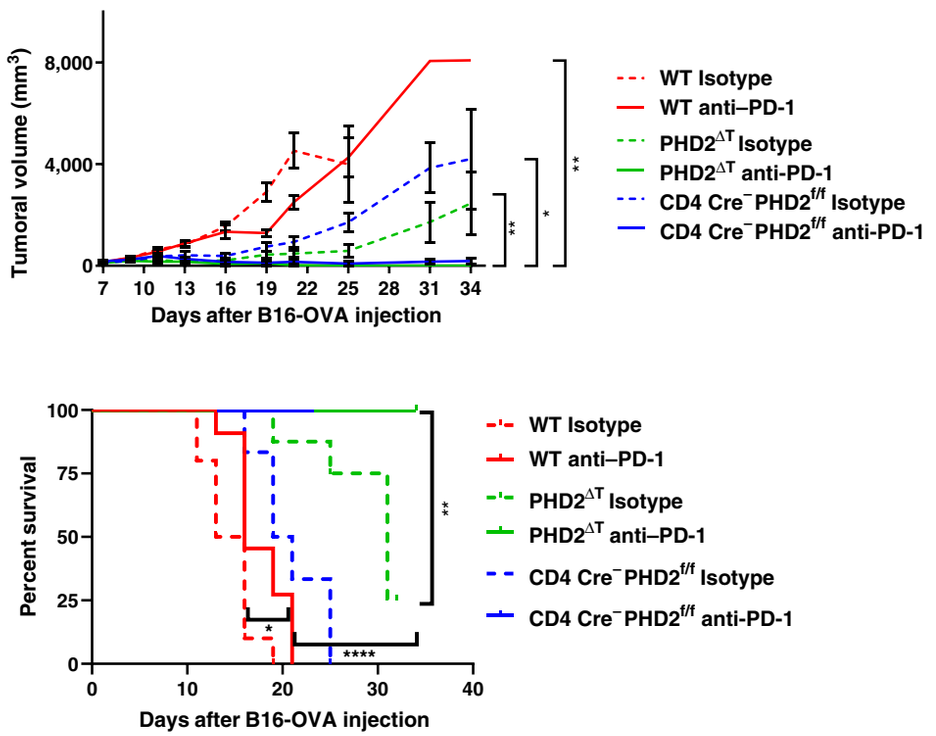

Figure 2.
Enhanced tumor regression in PHD2$^{\Delta T}$ mice treated with anti-PD-1 mAb. WT, CD4 Cre$^-$ PHD2$^{f/f}$, and PHD2$^{\Delta T}$ mice were injected subcutaneously with 5×10^5 B16-OVA tumor cells. Mice were treated with 200–280 μg anti-PD-1 or isotype control once each 2 days for 8 days. Tumor growth (top) and survival (bottom) were monitored each 3 days. Survival and growth data are from ($n = 16$) mice per group. Bars represent mean ± SD. Statistical significance for survival was determined by Log-rank (Mantel–Cox) test, and Wilcoxon test for tumor growth. *, $P < 0.05$; **, $P < 0.01$; ***, $P < 0.001$; ****, $P < 0.0001$; ns, not significant.

was strongly increased in tumor-infiltrating CD8$^+$ T cells from PHD2$^{\Delta T}$ mice, reaching about 40% of CD8$^+$ T cells (POP 1 and 2), as compared with 10% to 22% in other groups, whereas Granzyme B was overexpressed in POP 2 only, representing 15% of CD8$^+$ T lymphocytes (**Fig. 3B** and **C**). Concomitantly, the proportion of CD8$^+$ T lymphocytes expressing lower levels of four genes (POP 6) was strongly decreased. The absolute number of polyfunctional CD8$^+$ T lymphocytes per gram of tumor reached 41,000 in PHD2$^{\Delta T}$ mice, a 2-fold increase, as compared with 19,000 and 21,000 cells in WT and CD4 Cre$^-$ PHD2$^{fl/fl}$ mice, respectively (**Fig. 3D**).

A summary of all experiments performed (**Fig. 4A**) revealed that 36% of tumor-infiltrating CD8$^+$ T lymphocytes had the capacity to express IFNγ, TNFα, and Granzyme B in PHD2$^{\Delta T}$ mice, a more than 2-fold increase as compared with other groups. The calculation of the absolute numbers of cells showed a 6-fold selective increase in the number of CD8$^+$ T lymphocytes expressing these three cytotoxic-

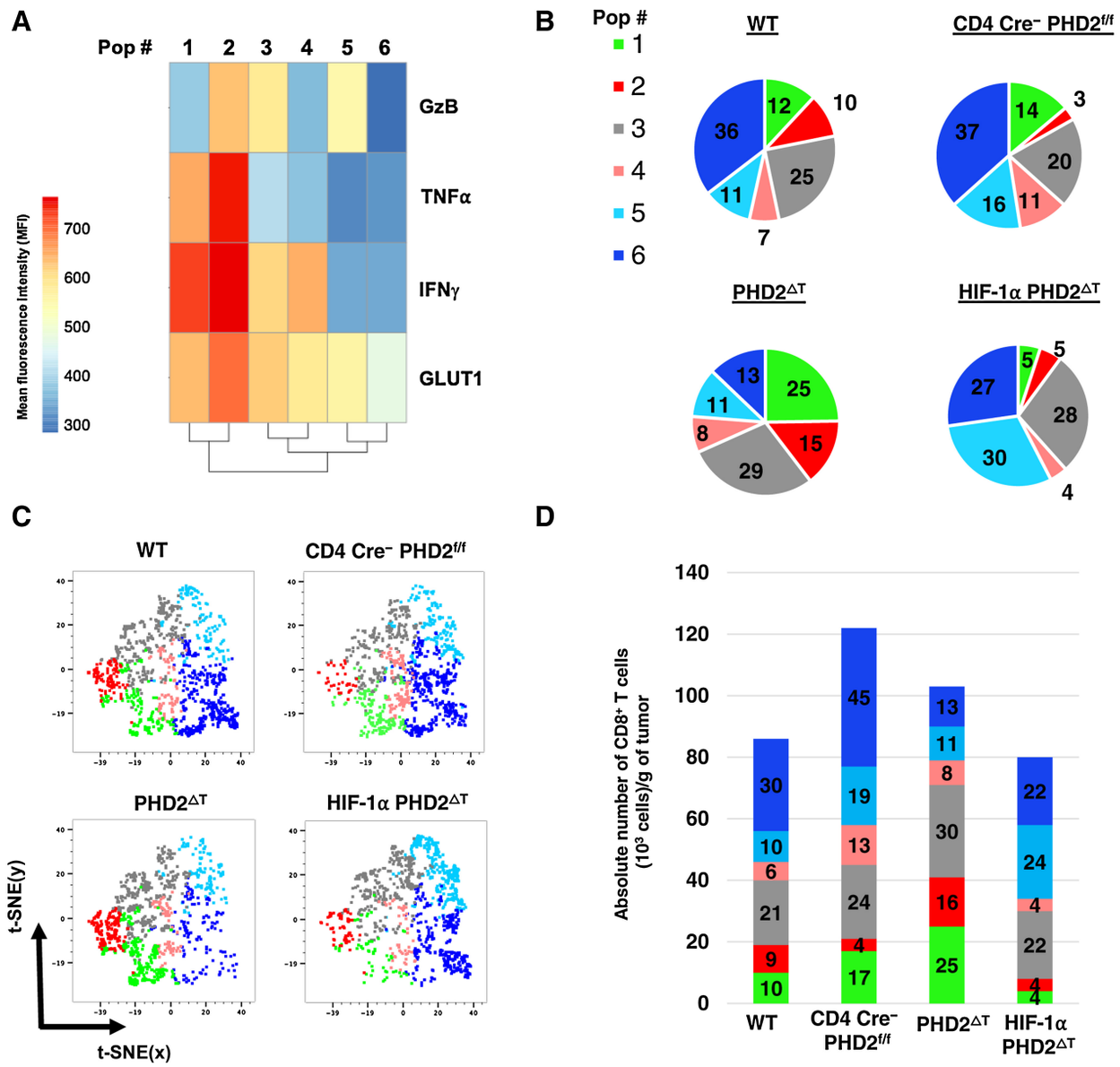

Figure 3.

Increased infiltration of polyfunctional CD8$^+$ T cells in tumors of PHD2$^{\Delta T}$ mice. WT, CD4 Cre$^-$ PHD2$^{f/f}$, PHD2$^{\Delta T}$, and HIF-1α PHD2$^{\Delta T}$ mice were injected subcutaneously with 10^6 EG7-OVA tumor cells. Tumors were harvested 13 to 14 days later and analyzed by flow cytometry. Unsupervised analysis of tumor-infiltrating CD8$^+$ T cells from 4 to 5 concatenated mice per group, using nonlinear dimensionality reduction in conjunction with t-distributed stochastic neighbor embedding (t-SNE) axes as inputs for clustering and FlowSOM cluster analysis. **A,** Heat map of the median fluorescence intensity (MFI) of IFNγ, TNFα, granzyme B, and GLUT1 for the 6 clusters; pie representation of the relative proportion of each cluster in each group (**B**); t-SNE graphs with the six clusters found by FlowSOM algorithm for each group (**C**) and absolute number per gram of tumor of each cluster of CD8$^+$ T cells infiltrating EG7-OVA tumor (**D**). Data are representative of three independent experiments with 3 to 6 mice per group.

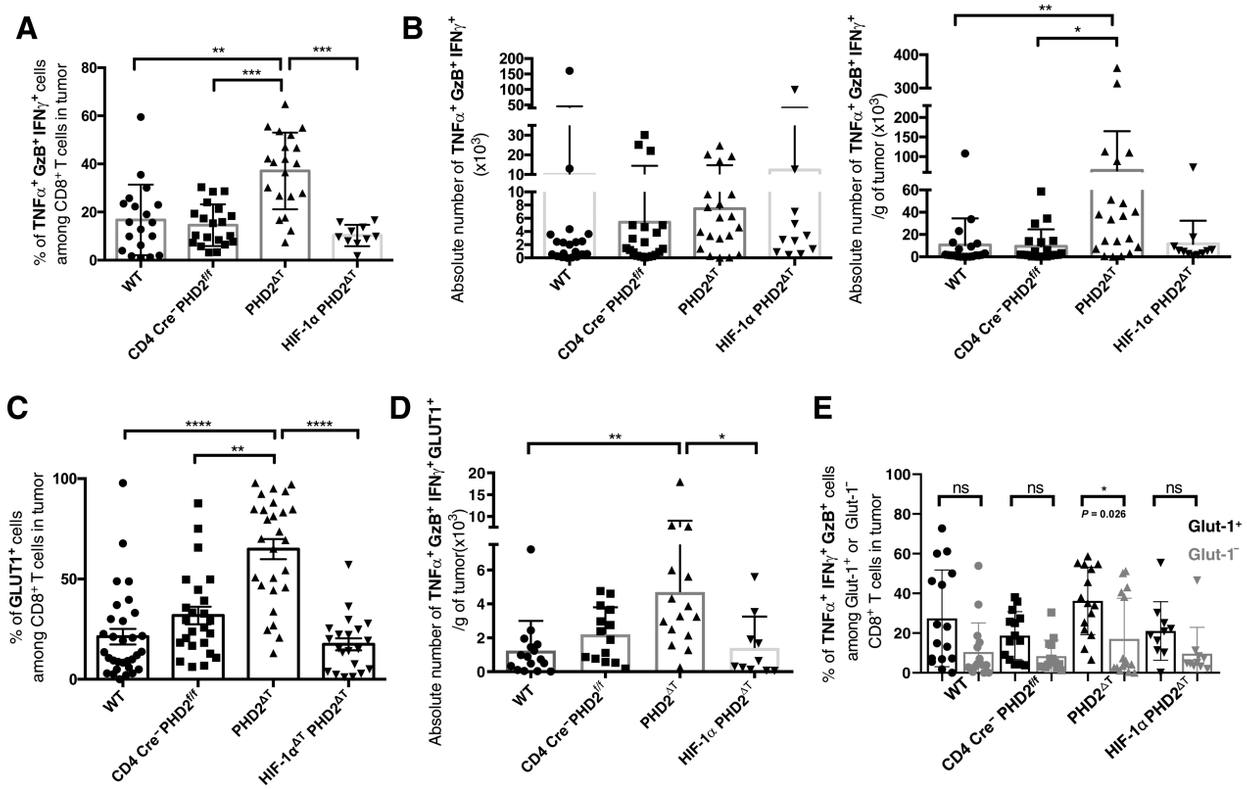

Figure 4.

Enhanced proportion of polyfunctional CD8$^+$ T cells in PHD2$^{\Delta T}$ mice. WT, CD4 Cre$^-$ PHD2$^{f/f}$, PHD2$^{\Delta T}$, and HIF-1α PHD2$^{\Delta T}$ mice were injected subcutaneously with 10^6 EG7-OVA tumor cells. Tumors were harvested 13 to 14 days later and analyzed by flow cytometry. **A–C,** Proportion (**A**), absolute number per tumor (**B**, left), or per gram of tumor (**B**, right) of IFNγ$^+$TNFα$^+$Granzyme B$^+$ cells infiltrating tumors. **C,** Proportion of GLUT1 expression among tumor-infiltrating CD8$^+$ T cells. **D,** Absolute number per gram of tumor of IFNγ$^+$TNF-α$^+$Granzyme B$^+$GLUT1$^+$ CD8$^+$ T cells. **E,** Proportion of polyfunctional cells among GLUT1$^+$ or GLUT1$^-$ CD8$^+$ T cells. Data are pooled from four ($n = 1$–6; **A** and **B**); six ($n = 3$–6; **C**); three ($n = 3$–6; **D** and **E**) independent experiments (each data point represents one mouse). Bars represent mean ± SD. Statistical significance was determined by Kruskal–Wallis multiple comparisons test. *, $P < 0.05$; **, $P < 0.01$; ***, $P < 0.001$; ****, $P < 0.0001$; ns, not significant.

associated factors in the same mice, reaching a mean of 65×10^3 per gram of tumor (**Fig. 4B**). The proportion of some cells expressing a single functional marker (TNFα) as well as dual expressors (IFNγ$^+$TNFα$^+$ and IFNγ$^+$Granzyme B$^+$) was also significantly increased in PHD2-deficient cells (Supplementary Fig. S4).

The glucose transporter GLUT-1 was expressed by 65% (mean of all experiments) of tumor-infiltrating CD8$^+$ T cells in PHD2$^{\Delta T}$ mice, as compared with 17% to 32% in other groups (**Fig. 4C**) and the absolute number of polyfunctional CD8$^+$ T lymphocytes expressing GLUT-1 was significantly increased in PHD2$^{\Delta T}$ mice, suggesting a potential role for glucose-dependent metabolism (**Fig. 4D**). In addition, the proportion of polyfunctional tumor-infiltrating CD8$^+$ T lymphocytes was higher among GLUT-1$^+$ than among GLUT-1$^-$ cells in PHD2$^{\Delta T}$ mice (**Fig. 4E**).

PHD2 regulates the exhaustion program of CD8$^+$ T lymphocytes

FACS analyses of tumor-infiltrating CD8$^+$ lymphocytes revealed a slight increase in KI67 expression in PHD2$^{\Delta T}$ mice, as compared with WT (Supplementary Fig. S5A) despite a similar effector memory phenotype, as assessed by CD44 and CD62 L expression (Supplementary Fig. S5B). However, expression of the transcription factor Eomes (as assessed by its relative frequency and mean fluorescence signal) was downregulated in PHD2-deficient cells (Supplementary Fig. S6A), an observation in line with a potential role for this transcription factor in cell exhaustion. RNA-seq data confirmed a 1.3-fold decrease in *Eomes* mRNA levels (see later discussion). The expression of *Tbx21* was not significantly different between groups.

We next used flow cytometry to examine the differentiation program of tumor-infiltrating CD8$^+$ T cells in PHD2$^{\Delta T}$ mice and CD4 Cre$^-$ *Phd2*$^{fl/fl}$ mice. The expression of several markers of differentiation/exhaustion revealed a change in the exhaustion program in PHD2$^{\Delta T}$ mice, i.e., an increased proportion of effector cells relative to "terminally exhausted" CD8$^+$ lymphocytes (**Fig. 5A**; ref. 25). Indeed, the major populations infiltrating the tumor in both strains of mice differed by their expression of PD-1, Tox, and Eomes, with a more than 2-fold decrease in the proportion of PD-1$^+$ cells among CD8$^+$ TILs (**Fig. 5B**). Among these PD-1$^+$ cells, we observed a decreased expression of the exhaustion-associated transcription factor TOX and a nonsignificant trend for increased proportion of TCF1$^+$TIM3^{lo} progenitor cells in PHD2$^{\Delta T}$ mice (**Fig. 5C**).

Finally, we evaluated the capacity of lymphocytes from PHD2$^{\Delta T}$ mice to acquire cytolytic activity independently of tumor growth. WT and PHD2$^{\Delta T}$ mice were primed by injection of OVA peptide–pulsed splenic dendritic cells and tested for cytotoxic activity *in vivo* 5 days later. The data in Supplementary Fig. S6B show a significant increase in the lysis of OVA-pulsed targets in PHD2$^{\Delta T}$ mice, as compared

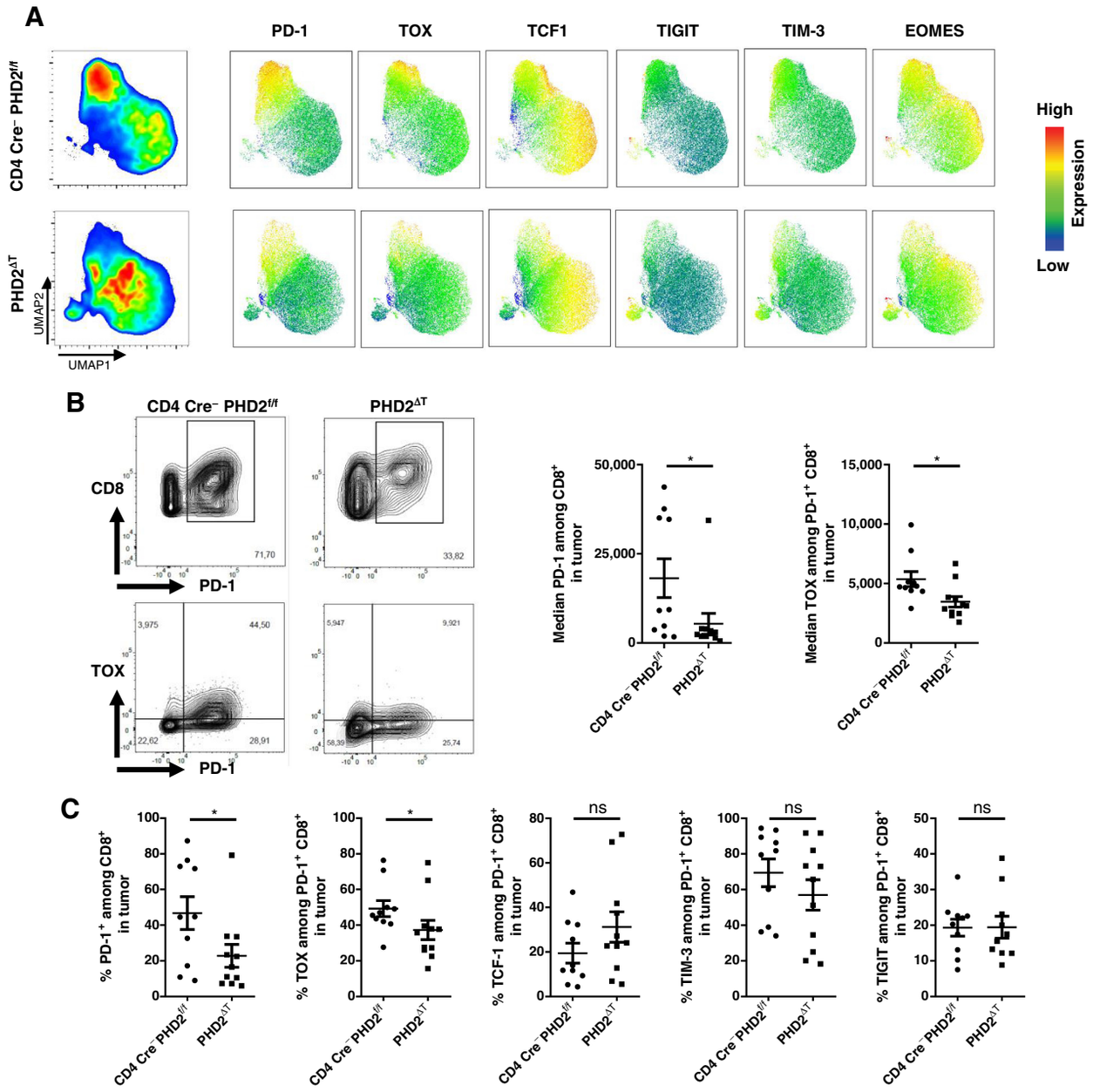

Figure 5.

Altered exhaustion program in TILs from PHD2$^{\Delta T}$ mice. CD4 Cre$^-$ PHD2$^{f/f}$ and PHD2$^{\Delta T}$ mice were injected subcutaneously with 10^6 EG7-OVA tumor cells. Tumors were harvested 10 days later and analyzed by flow cytometry. **A,** Uniform Manifold Approximation and Projection (UMAP) projection of data from CD8$^+$ T cells infiltrating tumors in CD4 Cre$^-$ PHD2$^{f/f}$ and PHD2$^{\Delta T}$ mice. The expression of each indicated marker is shown. Red indicates higher expression, blue indicates lower expression. **B,** Representative flow cytometry plots of indicated markers (left) and intensity (MFI) of PD-1 among tumor-infiltrating CD8$^+$ T cells and TOX among tumor-infiltrating CD8$^+$ T PD-1$^+$ cells (right). **C,** Percentage of PD-1$^+$ cells among tumor-infiltrating CD8$^+$ T cells, TOX, TCF-1, TIM-3, and TIGIT among PD-1$^+$. **B** and **C**, Data are pooled from two independent experiments ($n = 4$–5). Bars represent mean ± SD. Statistical significance was determined by unpaired *t* test. *, $P < 0.05$; ns, not significant.

with WT mice, suggesting that HIF-1α stabilization resulted in increased lytic activity of CD8$^+$ T cells even upon transient antigenic stimulation.

Collectively, these observations suggest that the stabilization of HIF-1α in T lymphocytes inhibits their differentiation from effector into terminally exhausted TOX^{hi}PD-1^{hi} cells, thereby favoring the recruitment, survival, and/or differentiation of polyfunctional CD8$^+$ T lymphocytes into the tumor bed.

Transcriptomic analysis

To gain insight into the mechanism underlying increased CD8$^+$ T-cell polyfunctionality in the context of PHD2 deficiency, we performed

RNA-seq analysis on CD8$^+$ T lymphocytes from WT and PHD2$^{\Delta T}$ mice 16 hours after anti-CD3 and anti-CD28 activation *in vitro*. We validated the PHD2 inactivation, as shown by the reduced frequency of reads coverage around exon 2 of the *Egln1* gene (**Fig. 6A**). Analysis of the dataset identified 19 downregulated genes and 132 upregulated upon PHD2 deletion (**Fig. 6B**). Among upregulated genes, were *Slc2a1* and *Slc2a3*, which encode for proteins (GLUT1 and GLUT3 respectively) that facilitate the transport of glucose. The representation analysis for pathways enriched from genes that were upregulated in activated CD8$^+$ T lymphocytes from PHD2$^{\Delta T}$ mice showed a specific enrichment of terms related to metabolism and energy (**Fig. 6C** and **D**). Several genes were involved in carbohydrate catabolic processes that generate pyruvate important for glycogenesis such as *Ldha*, *Aldoa, Pdk1*, and *Pgk1*. In addition, cytokine activity and regulation of immune effector process were strongly enriched implicating genes such as *Tbx21*, *Ifng*, *Irf7*, and *Bcl3*. Finally, genes such as *Vegfa*, *Rora*, and *Pdk1* enriched pathways related to hypoxia. These observations suggest a link between increased ability of tumor rejection and enhanced glycogenesis.

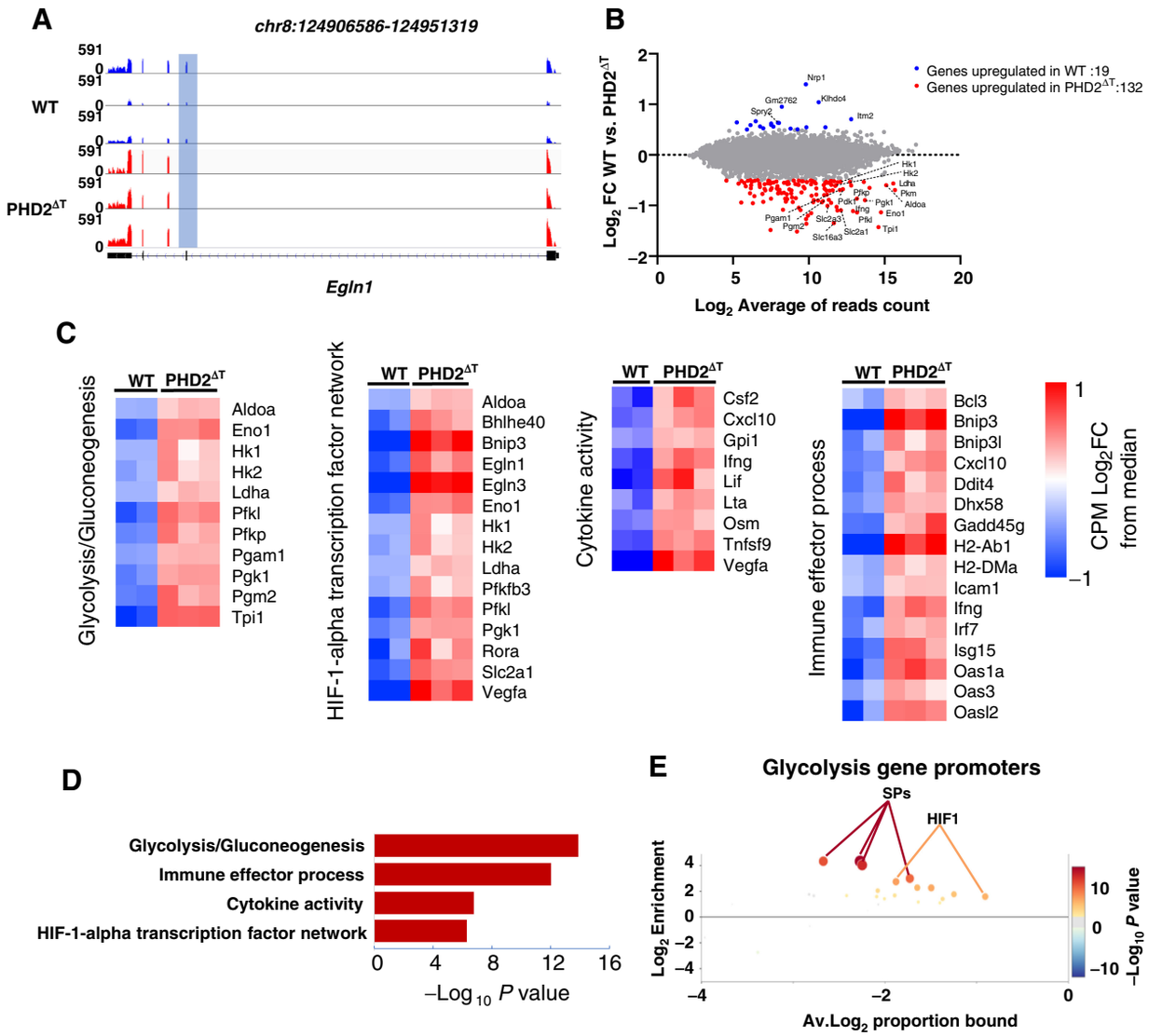

Figure 6.

Transcriptomic analysis of *in vitro* activated CD8$^+$ T cells. RNA-seq of CD8$^+$ T cells purified from WT and PHD2$^{\Delta T}$ spleen and activated *in vitro* with anti-CD3 plus anti-CD28 for 15 hours. **A,** Integrative Genomics Viewer tracks showing read coverage for RNA expression of *Egln1* gene in WT (blue) and Egln$^{\Delta T}$ (red). Gene position is indicated at the top of the panel. **B,** MA plot shows the fold change (log_2) versus average of read counts (log_2) (up in PHD2$^{\Delta T}$, red; up in WT, blue). **C,** Heat map representation of expression of transcripts involved in the glycolytic pathway, HIF-1α stabilization network, cytokine activity and immune effector function. The numbers of differentially expressed RNA are indicated. RNA-seq data were analyzed in triplicates for PHD2$^{\Delta T}$ and duplicate for WT. **D,** Gene ontology enrichment analysis of differentiated genes expressed in PHD2$^{\Delta T}$ CD8$^+$ T cells showing the enrichment *P* value expressed as $-log_{10}$. **E,** CiiiDER analysis of putative transcription factors motifs in promoter regions of glycolysis pathway shown in the heat map. Transcription factors are colored according to the *P* value of their gene coverage in CD8$^+$ T cells. The size of each point is also proportional to log_{10} *P* value.

To extend our understanding of PHD2 deletion on glycogenesis, we performed a motif enrichment analysis for transcription factors on the promoter of genes upregulated in CD8$^+$ T lymphocytes from PHD2$^{\Delta T}$ mice and associated with the glycogenesis process. We noticed a strong enrichment for HIF-1α motifs suggesting the involvement of this protein in the increased glycogenesis activity in these cells (**Fig. 6E**).

Aerobic glycolysis is required for enhanced differentiation of polyfunctional CD8$^{\pm}$ T lymphocytes in culture

On the basis of our observations and a previous report showing that aerobic glycolysis was required for cytokine production (but not activation and proliferation) by CD4$^+$ T lymphocytes (27), we compared the expression of cytokines in CD8$^+$ T lymphocytes cultured in either glucose (to engage aerobic glycolysis) or galactose (to enforce respiration). The data in **Fig. 7** indicate that the proportion of CD8$^+$ T lymphocytes expressing IFNγ and Granzyme B was higher in PHD2$^{\Delta T}$ mice than in WT or CD4 Cre$^-$ PHD2$^{\Delta T}$ counterparts, when activated in classical media (including glucose). Of note, culture in galactose-supplemented media led to a strong reduction in cytokine production and abrogated the difference among groups of mice. These data support the hypothesis that the increased function of CD8$^+$ T lymphocytes from PHD2$^{\Delta T}$ mice upon *in vitro* stimulation was dependent on glucose metabolism.

Genetic deletion of *phd2* in T lymphocytes improves PD-1 blockade immunotherapy

There is increasing evidence that cells expressing intermediate levels of PD-1 preferentially expand upon PD-1 blockade (28). We therefore explored the role of PHD2 in T lymphocytes in response to immunotherapy in the B16-OVA melanoma tumor model. We subcutaneously injected WT, control littermates (CD4 Cre$^-$ *Phd2*$^{fl/fl}$) and PHD2$^{\Delta T}$ mice with B16-OVA melanoma and treated them or not with anti–PD-1 at days 7, 9, 11, and 13. In WT mice, treatment with anti–PD-1 had a minor effect on tumor growth and survival (**Fig. 2**). In sharp contrast, tumors were completely rejected in PHD2$^{\Delta T}$ and CD4 Cre$^-$ *Phd2*$^{fl/fl}$ mice treated with anti–PD-1, indicating a strong synergism between PHD2 genetic deletion or hypomorphism and checkpoint blockade.

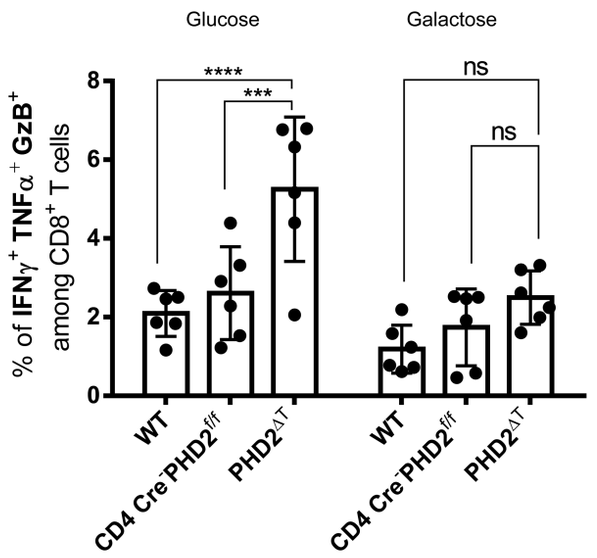

Figure 7.

Polyfunctionality is dependent on glucose metabolism. Splenic CD8$^+$ T cells were purified from WT, CD4 Cre$^-$ PHD2$^{f/f}$, and PHD2$^{\Delta T}$ mice and activated *in vitro* with anti-CD3 plus anti-CD28 in medium supplemented either with glucose (Glu) or galactose (Gal) for 15 hours and analyzed by flow cytometry. Data are pooled from three independent experiments ($n = 2$). Bars represent mean ± SD. Statistical significance was determined by two-way Anova with Dunnett multiple comparisons *post hoc* test. ***, $P < 0.001$; ****, $P < 0.0001$; ns, not significant.

Discussion

In this study, we show that the stabilization of HIF-1α in T lymphocytes (through genetic ablation of PHD2) enhanced the rejection of OVA-expressing tumors and altered the differentiation of CD8$^+$ T cells, preventing their progressive dysfunction. In particular, a larger number of effector/memory T lymphocytes, characterized by an increased capacity to express IFNγ, TNFα, and Granzyme B, infiltrated the regressing tumors in PHD2$^{\Delta T}$ mice. Of note, the stabilization of HIF-1α, even partial as in CD4 Cre$^-$ PHD2$^{fl/fl}$ mice, had a synergistic effect with anti–PD-1 therapy to control tumor growth and survival.

Our observations point to an elevated glycolytic metabolism induced by sustained HIF-1α signaling as a molecular mechanism by which HIF-1α yields more protective effector/memory CD8$^+$ T lymphocytes. Indeed, our data show: (i) an increased expression of the glucose transporter GLUT-1 by tumor-infiltrating CD8$^+$ T lymphocytes in PHD2$^{\Delta T}$ mice; (ii) a potent induction of genes related to glycolytic metabolism (glucose transporters GLUT-1/3 and rate limiting glycolytic enzymes) in PHD2-deficient CD8$^+$ T lymphocytes activated *in vitro*; (iii) the glucose dependency of the polyfunctional capacity (IFNγ, TNFα, and granzyme B production) of anti-CD3/CD28-stimulated PHD2-deficient CD8$^+$ T lymphocytes. This hypothesis is in line with data in the literature showing that oxidative phosphorylation (OXPHOS) and aerobic glycolysis interchangeably support T-cell proliferation/survival but that aerobic glycolysis is required for optimal IFNγ production in mice (27, 29) and humans (30). Accordingly, glucose deprivation was shown to limit the cytolytic function of effector CTL *in vitro* (31–33). Two *in vivo* studies have shown that constitutive HIF-dependent glycolytic metabolism (through conditional deletion of *Vhl* in T lymphocytes) enhances the effector responses of CD8$^+$ T lymphocytes and prevents exhaustion during chronic viral infection (20, 34). T-cell intrinsic deletion of PHD proteins was found to limit tumor colonization in the lung and improve adoptive cell transfer immunotherapy (35). Our data confirm these findings and further show that HIF-1α stabilization enhances the differentiation/recruitment of polyfunctional CD8$^+$ T lymphocytes *in vivo*, resulting in increased tumor rejection and cytotoxicity. In contrast, Mamlouk and colleagues (36) reported that loss of PHD2 in both T lymphocytes and myeloid cells was required for tumor regression, possibly due to macrophage-mediated immune subversion in their tumor model.

Our study may also explain the apparently paradoxical observation of a better survival rate in groups of patients with glioma and acute myeloid leukemia (AML) bearing tumors expressing a mutated allele of the gene encoding isocitrate dehydrogenase 1 [referred to as IDHmut tumors, see (37)]. Differential impact of IDH1/2 mutational subclasses on outcome in adult AML results from a large multicenter study (38). Although mutations in *IDH1* are often perceived as an immune evasion mechanism, it is noteworthy that gain-of-function mutations in this enzyme can lead to the accumulation of

2-hydroxyglutarate (2HG), a metabolite that can be produced as an L or a D enantiomer (39). Although both enantiomers can be considered as oncometabolites, their effect on immune cells are clearly distinguishable. In addition to promoting tumor development and fitness (39), D-2HG exerts potent immunosuppressive properties, notably by lowering the NAD/NADH ratio of tumor infiltrating $CD8^+$ T cells (40). Oncometabolite D-2HG alters T-cell metabolism to impair $CD8^+$ T-cell function (40). In marked contrast, L-2HG is known to inhibit PHD proteins leading to the stabilization of HIF-1α (41). S-2-hydroxyglutarate regulates $CD8^+$ T-lymphocyte fate (40, 41), leading to enhanced tumor infiltration and effector function, further confirming, in a clinical setting, the beneficial effect of HIF-1 stabilization during an antitumor response. In conclusion, whereas the hypoxia-derived L-2HG has been shown to affect PHD2 enzymatic activity, oncometabolites produced by IDHmut tumors appear to dysregulate the epigenetic program of both tumor and tumor-infiltrating cells independently of the PHD2–HIF-1α signaling pathway.

It is likely that the increased glucose transport in tumor-infiltrating $CD8^+$ T lymphocytes is of critical importance because of the metabolic competition in the tumor microenvironment (42, 43). Chang and colleagues have reported (44) that tumors may directly dampen the effector function of T lymphocytes by consuming glucose. They further show that programmed death-ligand 1 not only inhibits T lymphocytes via PD-1, but may also enhance tumor-cell glycolysis, thereby limiting glucose availability. Checkpoint blockade may therefore directly and indirectly potentiate T-cell function by increasing the level of available glucose in the tumor milieu. Of note, a recent report (45) confirmed that prolonged glucose restriction contributed to hyporesponsiveness of tumor-infiltrating $CD8^+$ T lymphocytes and further showed that acetate may restore IFNγ production in glucose-deprived T lymphocytes *in vitro* and *in vivo*.

We found a correlation between the superior tumor control and increased numbers of tumor-infiltrating $CD8^+$ T lymphocytes endowed with the capacity to produce IFNγ, TNFα, and granzyme B in $PHD2^{\Delta T}$ mice. These observations are consistent with several reports showing that polyfunctional $CD8^+$ T lymphocytes display a superior ability to reject tumor cells or control viral infections (46–51), a property lost by "exhausted" T cells. Among the mechanisms known to induce/maintain T-cell exhaustion during chronic infection, Eomes, a paralog of T-bet, and Sprouty 2 (*SPRY2*), a negative regulator of the MAPK/ERK pathway, may be of interest in our setting as they were decreased in PHD2-deficient $CD8^+$ T lymphocytes. The role of Eomes is complex, as it regulates both T-cell full differentiation and exhaustion, possibly depending on its level of expression (52). Li and colleagues reported that Eomes expression by tumor-infiltrating lymphocytes increased when tumor progressed and that Eomes was required for the development of antitumor effector cells. However, high levels of Eomes drove T lymphocyte unresponsiveness by inducing expression of T-cell exhaustion genes, such as *Havcr2* (which encodes TIM-3; ref. 52). Another study emphasized the complementary role of progenitor ($T\text{-bet}^+$) and terminal ($Eomes^+$) subsets of $CD8^+$ T lymphocytes to control viral infection (53). Accordingly, tumor-infiltrating $CD8^+$ T lymphocytes in $PHD2^{\Delta T}$ and control littermates differed by their expression of PD-1 and TOX. Furthermore, the decrease in SPRY2 expression in PHD2-deficient $CD8^+$ T lymphocytes (activated *in vitro*) may be relevant to the increased tumor control, as the lack of SPRY2 has been shown to enhance survival and T-cell polyfunctionality of effector $CD8^+$ T lymphocytes in mice (54, 55) and humans (56). This hypothesis is further supported by a report showing that HIF-1α and HIF-2α increased the methylation of the *SPRY2* promoter, leading to decreased *SPRY2* mRNA levels in a hepatoma cell line (57). Finally, our data show that neuropilin 1, a potential biomarker for dysfunctional T lymphocytes, was downregulated in $PHD2^{\Delta T}$ mice, suggesting a potential role as immune memory checkpoint (58, 59). Additional experiments will be required to clarify the role of these genes in the antitumor response of $PHD2^{\Delta T}$ mice.

Broadly, we conclude that the stabilization of HIF-1α in T lymphocytes regulates the metabolic balance within the tumor niche, favoring the differentiation of polyfunctional CTLs. In addition to a direct effect on aerobic glycolysis, the HIF complex has been shown to control expression of CTL effector molecules, trafficking (HIF-null cells retain the expression of lymph-node-homing receptors; ref. 32) and regulation of TCR signaling, suggesting that several mechanisms may contribute to the control of tumor growth in PHD2-deficient mice. There is now increasing evidence that hypoxia may have a beneficial effect on the antitumor function of $CD8^+$ T lymphocytes, thereby providing novel potential targets for cancer immunotherapy, eventually in association with currently available immune checkpoint blockers.

Authors' Disclosures

S. Goriely reports grants from Walloon Region, Fondation contre le cancer (Belgium); and grants from FNRS and Télévie during the conduct of the study. No disclosures were reported by the other authors.

Authors' Contributions

C. Bisilliat Donnet: Conceptualization, resources, investigation, methodology. **V. Acolty:** Resources, investigation, methodology. **A. Azouz:** Validation, investigation. **A. Taquin:** Investigation, methodology. **C. Henin:** Investigation, methodology. **S. Trusso Cafarello:** Investigation. **S. Denanglaire:** Investigation, methodology. **M. Mazzone:** Conceptualization, supervision, writing–review and editing. **G. Oldenhove:** Formal analysis, supervision. **O. Leo:** Conceptualization, supervision, validation, writing–review and editing. **S. Goriely:** Supervision, writing–review and editing. **M. Moser:** Conceptualization, resources, writing–original draft, writing–review and editing.

Acknowledgments

We are grateful to Peter Carmeliet (KU Leuven, Leuven, Belgium) for providing mice with *lox*P-flanked *Phd2* alleles and to Benoit Van den Eynde and Pierre Coulie (UCLouvain, Belgium) for interesting discussion and helpful suggestions. We thank Fabienne Andris and Kevin Englebert for valuable help, and Caroline Abdelaziz and Véronique Dissy for animal care.

The work was supported by the National Fund for Scientific Research (FNRS), the Fondation contre le Cancer, the Walloon Region (IMMUCAN), the European Regional Development Fund (ERDF-Wallonia BioMed 2014–2020-LIV 45–20), and grants from the Fonds Jean Brachet and the Fonds Hoguet.

The publication costs of this article were defrayed in part by the payment of publication fees. Therefore, and solely to indicate this fact, this article is hereby marked "advertisement" in accordance with 18 USC section 1734.

Note

Supplementary data for this article are available at Cancer Immunology Research Online (http://cancerimmunolres.aacrjournals.org/).

Received February 16, 2022; revised October 17, 2022; accepted January 3, 2023; published first January 5, 2023.

References

1. Traversari C. A nonapeptide encoded by human gene MAGE-1 is recognized on HLA-A1 by cytolytic T lymphocytes directed against tumor antigen MZ2-E. J Exp Med 1992;176:1453–7.
2. Coulie PG, Van den Eynde BJ, van der Bruggen P, Boon T. Tumor antigens recognized by T lymphocytes: at the core of cancer immunotherapy. Nat Rev Cancer 2014;14:135–46.
3. Hirota K. Basic biology of hypoxic responses mediated by the transcription factor HIFs and its implication for medicine. Biomedicines 2020;8:32.
4. Semenza GL. HIF-1, O2, and the 3 PHDs: minireview how animal cells signal hypoxia to the nucleus. Cell 2001;107:1–3.
5. Casazza A, Laoui D, Wenes M, Rizzolio S, Bassani N, Mambretti M, et al. Impeding macrophage entry into hypoxic tumor areas by Sema3A/Nrp1 signaling blockade inhibits angiogenesis and restores antitumor immunity. Cancer Cell 2013;24:695–709.
6. Chiu DKC, Xu IMJ, Lai RKH, Tse APW, Wei LL, Koh HY, et al. Hypoxia induces myeloid-derived suppressor cell recruitment to hepatocellular carcinoma through chemokine (C-C motif) ligand 26. Hepatology 2016; 64:797–813.
7. Thiel M, Caldwell CC, Kreth S, Kuboki S, Chen P, Smith P, et al. Targeted deletion of HIF-1α gene in T cells prevents their inhibition in hypoxic inflamed tissues and improves septic mice survival. PLoS One 2007;2:e853.
8. Higashiyama M, Hokari R, Hozumi H, Kurihara C, Ueda T, Watanabe C, et al. HIF-1 in T cells ameliorated dextran sodium sulfate-induced murine colitis. J Leukoc Biol 2012;91:901–9.
9. Georgiev P, Belikoff BG, Hatfield S, Ohta A, Sitkovsky MV, Lukashev D. Genetic deletion of the HIF-1α isoform I.1 in T cells enhances antibacterial immunity and improves survival in a murine peritonitis model: immunity to infection. Eur J Immunol 2013;43:655–66.
10. Westendorf AM, Skibbe K, Adamczyk A, Buer J, Geffers R, Hansen W, et al. Hypoxia enhances immunosuppression by inhibiting CD4+ effector T-cell function and promoting Treg activity. Cell Physiol Biochem 2017;41:1271–84.
11. Dang EV, Barbi J, Yang HY, Jinasena D, Yu H, Zheng Y, et al. Control of TH17/Treg balance by hypoxia-inducible factor-1. Cell 2011;146:772–84.
12. Shi LZ, Wang R, Huang G, Vogel P, Neale G, Green DR, et al. HIF-1α–dependent glycolytic pathway orchestrates a metabolic checkpoint for the differentiation of TH_{17} and Treg cells. J Exp Med 2011;208:1367–76.
13. Clambey ET, McNamee EN, Westrich JA, Glover LE, Campbell EL, Jedlicka P, et al. Hypoxia-inducible factor-1 alpha—dependent induction of FoxP3 drives regulatory T-cell abundance and function during inflammatory hypoxia of the mucosa. Proc Natl Acad Sci USA 2012;109:E2784–93.
14. Noman MZ, Desantis G, Janji B, Hasmim M, Karray S, Dessen P, et al. PD-L1 is a novel direct target of HIF-1, and its blockade under hypoxia enhanced MDSC-mediated T cell activation. J Exp Med 2014;211:781–90.
15. Curiel TJ, Wei S, Dong H, Alvarez X, Cheng P, Mottram P, et al. Blockade of B7-H1 improves myeloid dendritic cell–mediated antitumor immunity. Nat Med 2003;9:562–7.
16. Krishnamachary B, Zagzag D, Nagasawa H, Rainey K, Okuyama H, Baek JH, et al. Hypoxia-inducible factor-1—dependent repression of *E-cadherin* in von Hippel-Lindau tumor suppressor–null renal cell carcinoma mediated by TCF3, ZFHX1A, and ZFHX1B. Cancer Res 2006;66:2725–31.
17. Nishi H, Sasaki T, Nagamitsu Y, Terauchi F, Nagai T, Nagao T, et al. Hypoxia-inducible factor-1 mediates upregulation of urokinase-type plasminogen activator receptor gene transcription during hypoxia in cervical cancer cells. Oncol Rep 2016;35:992–8.
18. Wang B, Ding YM, Fan P, Wang B, Xu JH, Wang WX. Expression and significance of MMP2 and HIF-1α in hepatocellular carcinoma. Oncol Lett 2014;8:539–46.
19. Wong CCL, Gilkes DM, Zhang H, Chen J, Wei H, Chaturvedi P, et al. Hypoxia-inducible factor-1 is a master regulator of breast cancer metastatic niche formation. Proc Natl Acad Sci USA 2011;108:16369–74.
20. Doedens AL, Phan AT, Stradner MH, Fujimoto JK, Nguyen JV, Yang E, et al. Hypoxia-inducible factors enhance the effector responses of $CD8^+$ T cells to persistent antigen. Nat Immunol 2013;14:1173–82.
21. Palazon A, Tyrakis PA, Macias D, Veliça P, Rundqvist H, Fitzpatrick S, et al. An HIF-1α/VEGF-a axis in cytotoxic T cells regulates tumor progression. Cancer Cell 2017;32:669–83.
22. Gropper Y, Feferman T, Shalit T, Salame TM, Porat Z, Shakhar G. Culturing CTLs under hypoxic conditions enhances their cytolysis and improves their antitumor function. Cell Rep 2017;20:2547–55.
23. Mazzone M, Dettori D, Leite de Oliveira R, Loges S, Schmidt T, Jonckx B, et al. Heterozygous deficiency of PHD2 restores tumor oxygenation and inhibits metastasis via endothelial normalization. Cell 2009;136:839–51.
24. Stegen S, van Gastel N, Eelen G, Ghesquière B, D'Anna F, Thienpont B, et al. HIF-1α promotes glutamine-mediated redox homeostasis and glycogen-dependent bioenergetics to support postimplantation bone cell survival. Cell Metab 2016;23: 265–79.
25. Beltra JC, Manne S, A-H MS, Kurachi M, Giles JR, Chen Z, et al. Developmental relationships of four exhausted $CD8^+$ T cell subsets reveals underlying transcriptional and epigenetic landscape control mechanisms. Immunity 2020;52: 825–41.
26. Van Gassen S, Callebaut B, Van Helden MJ, Lambrecht BN, Demeester P, Dhaene T, et al. FlowSOM: Using self-organizing maps for visualization and interpretation of cytometry data: FlowSOM. Cytometry A 2015;87:636–45.
27. Chang CH, Curtis JD, Maggi LB, Faubert B, Villarino AV, O'Sullivan D, et al. Posttranscriptional control of T-cell effector function by aerobic glycolysis. Cell 2013;153:1239–51.
28. Blackburn SD, Shin H, Freeman GJ, Wherry EJ. Selective expansion of a subset of exhausted CD8 T cells by αPD-L1 blockade. Proc Natl Acad Sci USA 2008;105: 15016–21.
29. Cham CM, Gajewski TF. Glucose availability regulates IFN-γ production and p70S6 kinase activation in $CD8^+$ effector T cells. J Immunol 2005;174:4670–7.
30. Cretenet G, Clerc I, Matias M, Loisel S, Craveiro M, Oburoglu L, et al. Cell surface Glut1 levels distinguish human CD4 and CD8 T lymphocyte subsets with distinct effector functions. Sci Rep 2016;6:24129.
31. Cham CM, Driessens G, O'Keefe JP, Gajewski TF. Glucose deprivation inhibits multiple key gene expression events and effector functions in $CD8^+$ T cells. Eur J Immunol 2008;38:2438–50.
32. Finlay DK, Rosenzweig E, Sinclair LV, Feijoo-Carnero C, Hukelmann JL, Rolf J, et al. PDK1 regulation of mTOR and hypoxia-inducible factor-1 integrate metabolism and migration of $CD8^+$ T cells. J Exp Med 2012;209:2441–53.
33. MacDonald HR, Koch CJ. Energy metabolism and T-cell–mediated cytolysis. I. Synergism between inhibitors of respiration and glycolysis. J Exp Med 1977;146: 698–709.
34. Phan AT, Doedens AL, Palazon A, Tyrakis PA, Cheung KP, Johnson RS, et al. Constitutive glycolytic metabolism supports CD8 + T-cell effector memory differentiation during viral infection. Immunity 2016;45:1024–37.
35. Clever D, Roychoudhuri R, Constantinides MG, Askenase MH, Sukumar M, Klebanoff CA, et al. Oxygen sensing by T cells establishes an immunologically tolerant metastatic niche. Cell 2016;166:1117–31.
36. Mamlouk S, Kalucka J, Singh RP, Franke K, Muschter A, Langer A, et al. Loss of prolyl hydroxylase-2 in myeloid cells and T-lymphocytes impairs tumor development: Oxygen sensors in tumor immunology. Int J Cancer 2014;134:849–58.
37. Murugan AK, Alzahrani AS. Isocitrate dehydrogenase IDH1 and IDH2 mutations in human cancer: prognostic implications for gliomas. Br J Biomed Sci 2022;79:10208.
38. Middeke JM, Metzeler KH, Röllig C, Krämer M, Eckardt JN, Stasik S, et al. Differential impact of IDH1/2 mutational subclasses on outcome in adult AML: results from a large multicenter study. Blood Adv 2022;6:1394–405.
39. Du X, Hu H. The roles of 2-hydroxyglutarate. Front Cell Dev Biol 2021;9:651317.
40. Notarangelo G, Spinelli JB, Perez EM, Baker GJ, Kurmi K, Elia I, et al. Oncometabolite D-2HG alters T-cell metabolism to impair $CD8^+$ T-cell function. Science 2022;377:1519–29.
41. Tyrakis PA, Palazon A, Macias D, L KianL P AnthonyT, Veliça P, et al. S-2-hydroxyglutarate regulates $CD8^+$ T-lymphocyte fate. Nature 2016;540:236–41.
42. Renner K, Singer K, Koehl GE, Geissler EK, Peter K, Siska PJ, et al. Metabolic hallmarks of tumor and immune cells in the tumor microenvironment. Front Immunol 2017;8:248.
43. Lyssiotis CA, Kimmelman AC. Metabolic interactions in the tumor microenvironment. Trends Cell Biol 2017;27:863–75.
44. Chang CH, Qiu J, O'Sullivan D, Buck MD, Noguchi T, Curtis JD, et al. Metabolic competition in the tumor microenvironment is a driver of cancer progression. Cell 2015;162:1229–41.
45. Qiu J, Villa M, Sanin DE, Buck MD, O'Sullivan D, Ching R, et al. Acetate promotes T-cell effector function during glucose restriction. Cell Rep 2019;27: 2063–74.
46. Almeida JR, Price DA, Papagno L, Arkoub ZA, Sauce D, Bornstein E, et al. Superior control of HIV-1 replication by $CD8^+$ T cells is reflected by their avidity, polyfunctionality, and clonal turnover. J Exp Med 2007;204:2473–85.

47. Seder RA, Darrah PA, Roederer M. T-cell quality in memory and protection: implications for vaccine design. Nat Rev Immunol 2008;8:247–58.
48. Betts MR, Nason MC, West SM, Rosa SCD, Migueles SA, Abraham J, et al. HIV nonprogressors preferentially maintain highly functional HIV-specific $CD8^+$ T cells. Blood 2006;107:9.
49. Darrah PA, Patel DT, De Luca PM, Lindsay RWB, Davey DF, Flynn BJ, et al. Multifunctional TH1 cells define a correlate of vaccine-mediated protection against Leishmania major. Nat Med 2007;13:843–50.
50. Wimmers F, Aarntzen EHJG, Duiveman-deBoer T, Figdor CG, Jacobs JFM, Tel J, et al. Long-lasting multifunctional $CD8^+$ T-cell responses in end-stage melanoma patients can be induced by dendritic cell vaccination. Oncoimmunology 2016;5:e1067745.
51. Alfei F, Kanev K, Hofmann M, Wu M, Ghoneim HE, Roelli P, et al. TOX reinforces the phenotype and longevity of exhausted T cells in chronic viral infection. Nature 2019;571:265–9.
52. Li J, He Y, Hao J, Ni L, Dong C. High levels of Eomes promote exhaustion of antitumor $CD8^+$ T cells. Front Immunol 2018;9:2981.
53. Paley MA, Kroy DC, Odorizzi PM, Johnnidis JB, Dolfi DV, Barnett BE, et al. Progenitor and terminal subsets of $CD8^+$ T cells cooperate to contain chronic viral infection. Science 2012;338:1220–5.
54. Shehata HM, Khan S, Chen E, Fields PE, Flavell RA, Sanjabi S. Lack of Sprouty 1 and 2 enhances survival of effector $CD8^+$ T cells and yields more protective memory cells. Proc Natl Acad Sci USA 2018;115:E8939–47.
55. Collins S, Waickman A, Basson A, Kupfer A, Licht JD, Horton MR, et al. Regulation of $CD4^+$ and $CD8^+$ effector responses by Sprouty-1. PLoS One 2012;7:e49801.
56. Chiu YL, Shan L, Huang H, Haupt C, Bessell C, Canaday DH, et al. Sprouty-2 regulates HIV-specific T-cell polyfunctionality. J Clin Invest 2014;124:198–208.
57. Gao X, Hicks KC, Neumann P, Patel TB. Hypoxia-inducible factors regulate the transcription of the Sprouty2 gene and expression of the Sprouty2 protein. PLoS One 2017;12:e0171616.
58. Leclerc M, Voilin E, Gros G, Corgnac S, de Montpréville V, Validire P, et al. Regulation of antitumor CD8 T-cell immunity and checkpoint blockade immunotherapy by Neuropilin-1. Nat Commun 2019;10:3345.
59. Liu C, Somasundaram A, Manne S, Gocher AM, Szymczak-Workman AL, Vignali KM, et al. Neuropilin-1 is a T-cell memory checkpoint limiting long-term antitumor immunity. Nat Immunol 2020;21:1010–21.